Adjusted intensity nonlocal diffusion model of photopolymer grating formation

J. R. Lawrence

School of Physics and Astronomy, University of St. Andrews, North Haugh, St. Andrews KY16 9SS, Scotland

F. T. O'Neill

Department of Electronic and Electrical Engineering, University College Dublin, Belfield, Dublin 4, Republic of Ireland

J. T. Sheridan

Department of Electronic and Electrical Engineering, University College Dublin, Belfield, Dublin 4, Republic of Ireland

Received March 12, 2001; revised manuscript received August 13, 2001.

Diffusion-based models of grating formation in photopolymers have been proposed in which the rate of monomer polymerization (removal) is directly proportional to the illuminating intensity inside the medium. However, based on photochemical considerations, the rate of polymerization is proportional in the steady state to the square root of the interference intensity. Recently it was shown that, by introducing a nonlocal response function into the one-dimensional diffusion equation that governs holographic grating formation in photopolymers, one can deduce both high-frequency and low-frequency cutoffs in the spatial-frequency response of photopolymer materials. Here the first-order nonlocal coupled diffusion equations are derived for the case of a general relationship between the rate of polymerization and the exposing intensity. Assuming a two-harmonic monomer expansion, the resultant analytic solutions are then used to fit experimental growth curves for gratings fabricated with different spatial frequencies. Various material parameters, including monomer diffusion constant D and nonlocal variance σ, are estimated. © 2002 Optical Society of America

OCIS codes: 050.7330, 090.2900, 160.5470, 090.2890, 050.2770.

1. INTRODUCTION

Self-processing photopolymer materials enjoy widespread use as holographic recording media. Typically, illuminating light activates a dye, initiating polymerization, which drives a diffusion-based process.[1–7] The polymer chains grow away from their initiation points, removing monomers where they grow. It was recently proposed[8] that one can model this situation by introducing a nonlocal response function into the one-dimensional diffusion equation[9] that governs grating formation.[10,11] The physical extent of the nonlocal response is indicated by a normalized nonlocal variance σ, where $\sigma = 0$ and $\sigma > 0$ correspond to the local and the nonlocal cases, respectively. The variance quantifies the effects of polymer chain growth initiated at one point in the medium on the polymerization that takes place some distance away. The nonlocal diffusion model predicts the existence of both a high- and a low-frequency cutoff in the material's spatial frequency response.

In Refs. 8, 10, and 11 it was assumed that the change in monomer concentration is directly proportional to the recording interference pattern's intensity. An extension of the local diffusion model[12] uses a general relationship between the illuminating intensity and the polymerization rate. In a recent paper, starting with the physical analysis of Odian,[13] Kwon *et al.*[14] derived a rate of polymerization that is directly proportional to the square root of the illuminating intensity. In the present paper we examine the dependence of the square root on exposure intensity and incorporate it into the coupled harmonic nonlocal model. The resultant corrected model, model II, and the uncorrected model, model I, are then compared.

We derive approximate analytic solutions to the nonlocal diffusion equation, assuming a two-harmonic expansion of the monomer concentration. These analytic expressions are compared with the more rigorous four-harmonic numerical results, indicating the range of physical parameters for which they are accurate. The predictions of the model, corrected to allow for Fresnel reflections during recording and replay, are then compared with growth curves that we produced by measuring the diffraction intensities produced by volume holographic gratings with different spatial frequencies.

The holographic gratings used were all recorded in an acrylamide-based photopolymer material.[15–18] We calculated the resultant diffraction efficiencies, allowing for Fresnel boundary losses. By applying Kogelnik's coupled-wave theory,[4,7,19,20] we calculated the corresponding refractive-index modulations. Fitting these curves by using the two-harmonic analytic expressions, we estimated the bulk physical parameters that govern the behavior of the material. These parameters included the monomer diffusion constant D, the rate of polymerization F_0, the constant of proportionality between the exposure

0740-3224/2002/040621-09$15.00

energy and the rate of polymerization κ, the constant of proportionality between the polymer concentration and the resultant refractive index C, the dimensionless reaction rate R, and the normalized nonlocal polymer chain length distribution variance σ.[7] The trends in the behavior of these parameters as the spatial frequency is changed are indicated.

2. MODELING PHOTOCHEMICAL PROCESSES

Photopolymer systems use a sensitizer Z to initiate polymerization. The sensitizer (dye) absorbs light and moves into an excited state, Z^*. Typically this excited state then transfers its energy to another compound, C, which then becomes excited, C^*. Free radicals $R^\bullet$ are then formed by the decomposition of C^*. The mechanism for free-radical polymerization has three stages, namely, initiation, propagation, and termination. Initiation involves the production of free radicals, which bind to a monomer to form the chain-initiation species $M_1^\bullet$:

$$R^\bullet + M \overset{k_i}{\rightarrow} M_1^\bullet, \tag{1}$$

where k_i is the initiation rate constant. The radical $M_1^\bullet$ then propagates by bonding with other monomer molecules to form a long polymer chain:

$$M_n^\bullet + M \overset{k_p}{\rightarrow} M_{n+1}^\bullet, \tag{2}$$

where k_p is the propagation rate constant. The growth of the polymer chain is stopped by termination. Termination occurs when the radical attached to the end of the growing polymer chain bonds with a free radical. This reaction produces a dead polymer, i.e., a chain with no radical attached to one end and which is therefore incapable of growing further:

$$M_n^\bullet + M_m^\bullet \overset{k_t}{\rightarrow} \text{dead polymer}, \tag{3}$$

where k_t is the termination rate constant. Normally the rate of termination is higher than the rate of propagation. However, the concentration of free radicals is much lower than the concentration of monomers, so the polymer chain can grow for some time before it is terminated.

The rate of disappearance of monomers can be given by

$$-\frac{\partial c}{\partial t} = R_i + R_p, \tag{4}$$

where c is the monomer concentration, R_i is the initiation rate, and R_p is the rate of propagation. Because there is a larger number of monomers than free radicals, it can be assumed that $R_p \gg R_i$.[12] Therefore Eq. (4) can be rewritten as

$$-\frac{\partial c}{\partial t} = R_p. \tag{5}$$

The rate of polymerization can be given by

$$R_p = k_p c c_r, \tag{6}$$

where c_r is the total concentration of chain radicals. The radical concentration rises exponentially at first, reaching a steady state that is maintained during the polymerization. This reaching of steady state implies that the rate of initiation, R_i, and the rate of termination, R_t, are equal, yielding

$$R_i = R_t = 2k_t {c_r}^2. \tag{7}$$

The expression for c_r is substituted into Eq. (6) to give the rate of polymerization:

$$R_p = k_p c (R_i/2k_t)^{1/2} \propto {R_i}^{1/2}. \tag{8}$$

Clearly the rate of propagation is proportional to the square root of the initiation rate. The initiation rate is $R_i = 2\Phi I_a$, where Φ is the quantum yield of radical production, which can be defined as the number of pairs of radicals formed per quantum of light absorbed.[13] I_a is the intensity of light absorbed, expressed in moles of light quanta per liter per second. Given that the spatially modulated illumination is $I(x) = I_0[1 + V\cos(Kx)]$, where V is the visibility and the grating vector magnitude is $K = 2\pi/\Lambda$, where Λ is the grating period, I_a is

$$I_a(x) = I(x)[1 - \exp(-\varepsilon Z d)] = I(x)(1 - T), \tag{9}$$

where ε is the molar absorptivity, Z is the concentration of photosensitizers, d is the thickness of the photopolymer layer, and T is the transmittance of the layer. When the initiation step is started by the photosensitizers, the concentration of the radicals can be given by

$$c_r = \left[\frac{\Phi I(x)(1 - T)}{k_t}\right]^{1/2}, \tag{10}$$

and the polymerization rate, Eq. (6), is given by

$$R_p = k_p c\left[\frac{\Phi I(x)(1 - T)}{k_t}\right]^{1/2}. \tag{11}$$

Combining Eqs. (5) and (11) yields the rate of polymerization of the monomers:

$$-\frac{\partial c}{\partial t} = k_p c\left[\frac{\Phi I(x)(1 - T)}{k_t}\right]^{1/2}. \tag{12}$$

As we stated above, monomers diffuse from dark regions to bright regions as the concentration of monomers is modulated by the illumination. This diffusion equation[13] can be combined with Eq. (11) to give the monomer concentration:

$$-\frac{\partial c}{\partial t} = D\frac{\partial^2 c}{\partial x^2} + Q[1 + V\cos(Kx)]^{1/2} c, \tag{13}$$

where

$$Q = k_p\left[\frac{\Phi I_0(1 - T)}{k_t}\right]^{1/2}$$

is analogous to F_0 as it appears in Refs. 10 and 11. Parameters κ in Ref. 8 and $k_p\{[\Phi(1 - T)]/k_t\}^{1/2}$ in Ref. 14 are similarly analogous.

3. NONLOCAL MATERIAL RESPONSE

In this section we incorporate the square root dependence into the nonlocal model. Recall the one-dimensional nonlocal response diffusion equation[8]:

$$\frac{\partial u(x,\,t)}{\partial t} = \frac{\partial}{\partial x}\left[D(x,\,t)\,\frac{\partial u(x,\,t)}{\partial x}\right] - \int_{-\infty}^{+\infty} R(x,\,x')F(x',\,t)u(x',\,t)\mathrm{d}x'. \tag{14}$$

Assume a monomer concentration given by

$$u(x',\,t') = \sum_{i=0}^{\infty} u_i(t)\cos(iKx') \tag{15}$$

and a diffusion constant expanded as

$$D(x,\,t) = \sum_{i=0}^{+\infty} D_i(t)\cos(iKx). \tag{16}$$

A Gaussian form of nonlocal material response function is chosen[8]:

$$R(x - x') = \frac{\exp[-(x - x')^2/2\sigma]}{\sqrt{2\pi\sigma}}. \tag{17}$$

Previously it was assumed that the rate of polymerization was of the form[8,10]

$$F(x',\,t) = F_0[1 + V\cos(Kx')]. \tag{18}$$

Equation (18) is used in model I.

This equation must now be adjusted to take account of the proposed dependence on the square root of intensity:

$$F(x',\,t) = F_0[1 + V\cos(Kx')]^{1/2}. \tag{19}$$

Equation (19) is used in model II.

Based on our definition of Q we define $F_0 = \kappa I_0^{1/2}$, where $\kappa = k_p\{[\Phi(1 - T)]/k_t\}^{1/2}$. $F(x,\,t)$ can be represented as a Fourier series:

$$F(x',\,t) = F_0\sum_{i=0}^{\infty} f_i\cos(iKx'). \tag{20}$$

We substitute Eqs. (15)–(17) and (20) into Eq. (14) to give the first-order nonlocal coupled equations that govern the time evolution of the harmonics of monomer concentration for any intensity-dependent rate of polymerization and the diffusion constant:

$$\frac{\mathrm{d}u_0(t)}{\mathrm{d}t} = -F_0f_0u_0(t) - \frac{F_0}{2}\sum_{n=1}^{\infty} f_nu_n(t), \tag{21a}$$

$$\left.\frac{\mathrm{d}u_j(t)}{\mathrm{d}t}\right|_{j>0} = -(jK)^2D_0(t)u_j(t) - j\frac{K^2}{2}\sum_{n=1}^{j-1} nD_{j-n}(t)u_n(t) - F_0f_0u_j(t) \times \exp[-(jK)^2\sigma/2] - \frac{F_0\exp[-(jK)^2\sigma/2]}{2}\left[\sum_{i=0}^{+\infty} f_{j+i}u_i(t) + \sum_{i=1+j}^{+\infty} f_{i-j}u_i(t) + \sum_{i=0}^{j-1} f_{j-i}u_i(t)\right] + j\frac{K^2}{2}\sum_{n=1}^{+\infty}[nD_{n+j}(t)u_n(t) - (n + j)D_n(t)u_{n+j}(t)]. \tag{21b}$$

Several assumptions are now made.[8,10,12] It is assumed that, in the Fourier series expansion of the diffusion constant, only the first two terms must be retained:

$$D(x,\,t) = D\exp[-\alpha F_0t(\sqrt{1 - V} + \sqrt{1 + V})/2] \times \left\{\cosh\left[\frac{\alpha F_0t(\sqrt{1 + V} - \sqrt{1 - V})}{2}\right] - \sinh\left[\frac{\alpha F_0t(\sqrt{1 + V} - \sqrt{1 - V})}{2}\right]\cos(Kx)\right\}. \tag{22}$$

This assumption was examined previously and was shown to be acceptable, because the first or average term dominates, except in cases of high nonlinearity.[10] The diffusion constant is assumed to decay exponentially as a function of the polymerization rate, where α is the diffusion constant's decay parameter.[10] We also introduce ξ, which is proportional to the rate of polymerization:

$$\xi = F_0t = \kappa I_0{}^{1/2}t. \tag{23}$$

We substitute from Eqs. (22) and (23) into Eqs. (21). Assuming that the monomer concentration profile is well approximated by a four-harmonic series, i.e., that $u_{i>3}(\xi) = 0$ and that $f_{m>5} = 0$, the four coupled monomer rate equations are

$$\frac{\mathrm{d}u_0(\xi)}{\mathrm{d}\xi} = -f_0u_0(\xi) - \frac{1}{2}[f_1u_1(\xi) + f_2u_2(\xi) + f_3u_3(\xi)], \tag{24a}$$

$$\frac{du_1(\xi)}{d\xi} = -R\,\mathrm{Ch}[\xi]u_1(\xi) - R\,\mathrm{Sh}[\xi]u_2(\xi) - S_1\left[f_1u_0(\xi) + \left(f_0 + \frac{f_2}{2}\right)u_1(\xi) + \frac{1}{2}(f_1 + f_3)u_2(\xi) + \frac{1}{2}(f_2 + f_4)u_3(\xi)\right], \tag{24b}$$

$$\frac{du_2(\xi)}{d\xi} = -4R\,\mathrm{Ch}[\xi]u_2(\xi) + R\,\mathrm{Sh}[\xi][u_1(\xi) + 3u_3(\xi)] - S_2\left[f_2u_0(\xi) + \frac{1}{2}(f_0 + f_2)u_1(\xi) + \left(f_0 + \frac{f_4}{2}\right)u_2(\xi) + \frac{1}{2}(f_1 + f_5)u_3(\xi)\right], \tag{24c}$$

$$\frac{du_3(\xi)}{d\xi} = -9R\,\mathrm{Ch}[\xi]u_3(\xi) + 3R\,\mathrm{Sh}[\xi]u_2(\xi) - S_3\left[f_3u_0(\xi) + \frac{1}{2}(f_2 + f_4)u_1(\xi) - \frac{1}{2}(f_1 + f_5)u_2(\xi) - \left(f_0 + \frac{f_6}{2}\right)u_3(\xi)\right], \tag{24d}$$

where $\mathrm{Ch}[\xi] = \exp[-\alpha F_0 t(\sqrt{1-V} + \sqrt{1+V})/2] \times \cosh[\alpha F_0 t(\sqrt{1+V} - \sqrt{1-V})/2]$, $R = DK^2/F_0$, $S_i = \exp(-i^2K^2\sigma/2)$, and $\mathrm{Sh}[\xi] = \exp[-\alpha F_0 t(\sqrt{1-V} + \sqrt{1+V})/2]\sinh[\alpha F_0 t(\sqrt{1+V} - \sqrt{1-V})/2]$.

Equations (24) are solved numerically[21] with the initial conditions $u_0(0) = 100$ and $u_m(0) = 0$ for all $m > 0$. When $V = 1$, $f_0 = 2\sqrt{2}/\pi$ and

$$f_m = \frac{4\sqrt{2}}{\pi}\frac{(-1)^{m+1}}{(-1 + 4m^2)}.$$

When the square root is eliminated, the equations reduce to model I[8] and $f_0 = 1$, $f_1 = V$, and $f_{m>1} = 0$.

4. ANALYTIC FORMULAS FOR MODEL II

We derived analytic expressions for monomer and polymer concentrations, assuming that the concentration was well approximated by the zeroth and first harmonics alone, (u_0 and u_1). To do so, we assumed that $\alpha = 0$, which we could do because changing α is equivalent to varying R (Ref. 10):

$$\frac{du_0(\xi)}{d\xi} = -f_0u_0(\xi) - f_1u_1(\xi)/2, \tag{25a}$$

$$\frac{du_1(\xi)}{d\xi} = -Sf_1u_0(\xi) - Wu_1(\xi), \tag{25b}$$

with $W = S(f_0 + f_2/2) + R$ and $S = S_1 = \exp(-K^2\sigma/2)$.

The analytic solutions to Eqs. (25) are of the form

$$u_0(\xi) = \frac{100\exp[(W + f_0)\xi/2]}{B}[B\cosh(B\xi/2) + (W - f_0) \times \sinh(B\xi/2)], \tag{26a}$$

$$u_1(\xi) = -\frac{100Sf_1}{B}\exp\left[-\frac{(B + W + f_0)\xi}{2}\right]\left[\exp\left(\frac{B\xi}{2}\right) - 1\right], \tag{26b}$$

where $B = [(W - f_0)^2 + 2f_1^2S]^{1/2}$.

The resultant concentration of polymerized monomers[8,10] after an exposure of duration t s is given by

$$N(x, t) = \int_0^t\int_{-\infty}^{+\infty} R(x - x')F(x', t')u(x', t')\mathrm{d}x'\mathrm{d}t', \tag{27}$$

yielding the following polymerization concentration spatial-harmonic components:

$$N_0(\xi) = \int_0^\xi [f_0u_0(\xi') + (f_1/2)u_1(\xi')]\mathrm{d}\xi', \tag{28a}$$

$$N_1(\xi) = S\int_0^\xi [f_1u_0(\xi') + (f_0 + f_2/2)u_1(\xi')]\mathrm{d}\xi'. \tag{28b}$$

Substituting for u_0 and u_1 gives that

$$N_0(\xi) = 100 + \frac{50}{B}\exp\left[\frac{(W - f_0 - B)\xi}{2}\right]\left[(W - f_0 - B) - (W - f_0 + B)\exp\left[\frac{B\xi}{2}\right]\right], \tag{29a}$$

$$N_1(\xi) = \frac{400S}{B^2 - (W + f_0)^2}\left\{R + \exp\left[-\frac{(W + f_0)\xi}{2}\right] \times\left[\left(\frac{L}{B}\right)\sinh\left(\frac{B\xi}{2}\right) - R\cosh\left(\frac{B\xi}{2}\right)\right]\right\}, \tag{29b}$$

where $L = (f_0 - R)R + [-f_1^2 + (f_0 + f_2)(2f_0 - R)]S$.

It is assumed that the modulation of the refractive index induced during recording is linearly related to the polymer concentration. Therefore the change in cross-sectional refractive index recorded in the material is

$$n(x, \xi) = C\sum_{i=0}^{1} N_i(\xi)\cos(iKx). \tag{30}$$

5. COMPARISON OF MODELS I AND II

A numerical comparison of four-harmonic models I and II presented in Section 3 is carried out. For a consistent comparison we set $R(\mathrm{I}_1) = R(\mathrm{II}_1)$, i.e., we assume that $\kappa I_0|_{\text{model I}} = \kappa I_0^{1/2}|_{\text{model II}}$, in which case $\xi(\mathrm{I}_1) = \xi(\mathrm{II}_1)$. Therefore we assume that we are comparing two different media, which respond differently to the illuminating light

pattern. The predicted monomer and polymer concentration amplitudes and the corresponding grating profiles were examined. The R and S values that were used distinguish previously identified regimes of material behavior.[8,10]

Figure 1 shows the exposure-curve values of the zeroth harmonic (u_0) and the first harmonic (u_1) of monomer concentration predicted by model II (dashed curves) and by model I (solid curves). In fact, Fig. 1 shows the largest difference between the predictions (as we discuss below). The values of u_0 and u_1 predicted by model II follow the same general trends as were observed for model I[8]; i.e., as σ is increased, the monomer concentration falls off more rapidly and the amplitude of the higher harmonics is reduced.

Figure 2 shows an example of the differences in the zeroth (N_0) and first (N_1) harmonics of polymer concentration as predicted by the model I (solid curves) and by model II (dashed curves).

From Figs 1 and 2 it would appear that for $\xi > 10$ the system has effectively reached its final state, as no monomer remains to be polymerized. Therefore, fixing $\xi = 12$, in Figs. 3(a) and 3(b) we plot the numerical four-harmonic predictions for N_1 over the ranges $0.1 < S < 1$ and $0.01 < R < 100$ for models I and II, respectively. In both cases the strongest first-harmonic prediction occurs for a medium that has large $R = 100$ and large $S = 1$ values. This type of medium corresponds to a recording medium that is illuminated (intensity and period) such as to exhibit a high rate of diffusion (large D) and a low rate of polymerization (small F_0) and with short polymer chains (small σ). For both Figs. 3(a) and 3(b) the N_1 component drops to less than 10% of the maximum value (in the range) when $S < 0.2$ (for all R) and $R < 0.1$ (for all S). A comparison of the relative sizes of

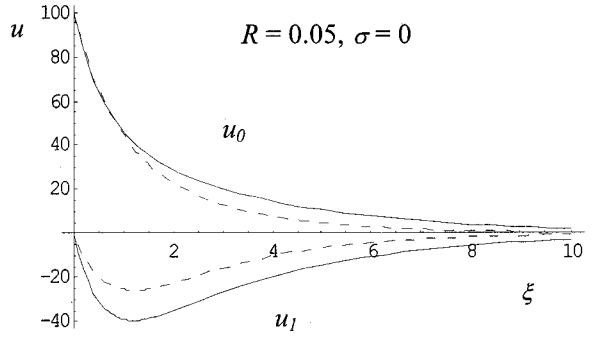

Fig. 1. Largest difference between u_0 and u_1 predicted by models I (solid curves) and II (dashed curves).

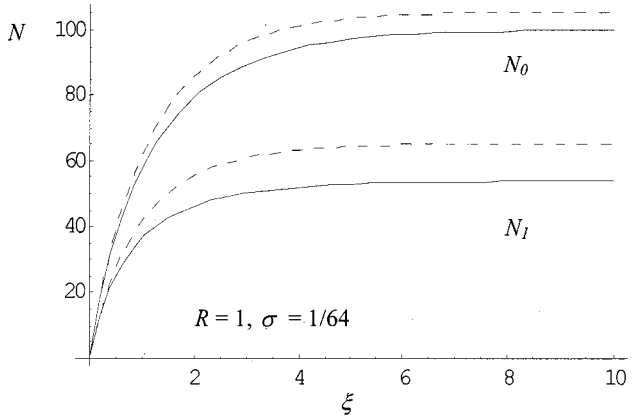

Fig. 2. Polymer concentration predicted by models I (solid curves) and II (dashed curves).

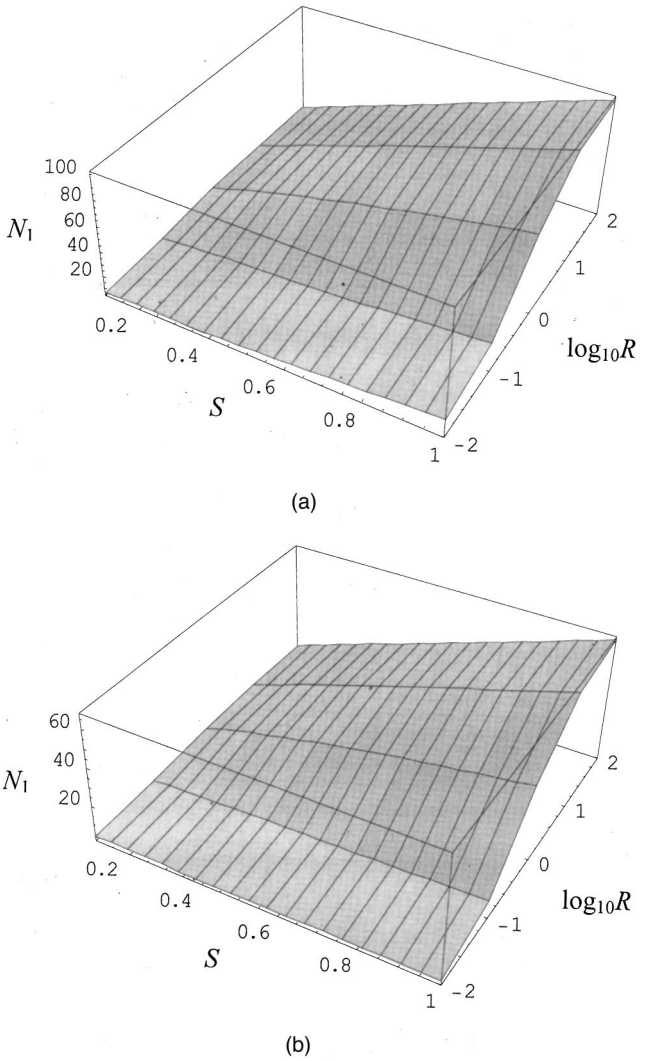

Fig. 3. (a) Model I: numerical four-harmonic N_1 result as a function of $0.1 < S < 1$ and $-2 < \log_{10}(R) < 2$ for $\xi = 12$. (b) Model II: numerical four-harmonic N_1 result for $\xi = 12$.

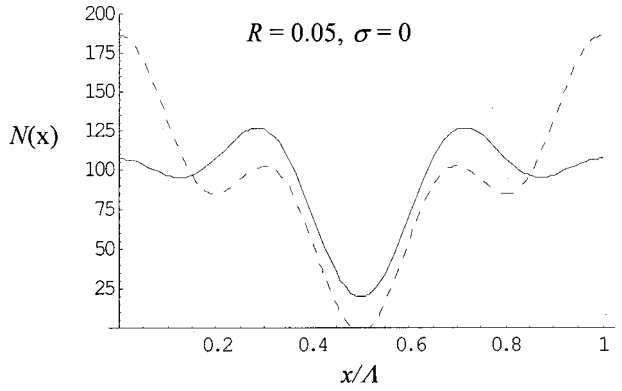

Fig. 4. Greatest difference between four-harmonic predictions, $\xi = 10$, of models I (solid curve) and II (dashed curve).

the predictions of the two models shows that, as R and σ increase, the two predictions became more similar in size.

Figure 4 shows the resultant cross-sectional polymer concentration profiles for the largest differences between the two models (and between the illuminating intensity and the resultant recorded profile) as predicted by four-harmonic model I (solid curve) and four-harmonic model II (dashed curve). In this case $V = 1$ and $\xi = 10$. The model II profile predictions follow the same trend as that for four-harmonic nonlocal model I,[8] i.e., (1) as R increases, the profiles become more sinusoidal in shape, and (2) increasing σ smooths the profile but decreases its visibility. For all values of R and σ examined, the visibility of the model II profile was found to be greater than that of the corresponding model I profile. The difference decreases as R and σ increase.

6. ACCURACY OF THE ANALYTIC FORMULAS

To quantify the accuracy of the two-harmonic model I and model II analytic formulas we define a percentage difference calculated from the formula

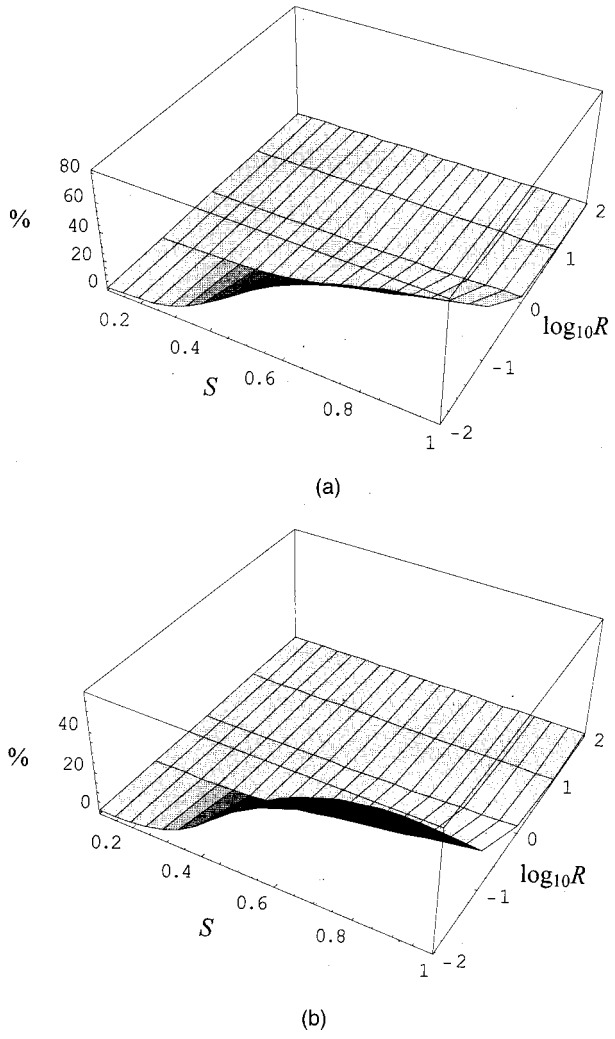

Fig. 5. Percentage difference between analytic formula and the numerical result for $\xi = 12$ for (a) model I and (b) model II.

$$\% = \frac{N_1(4 - \text{harmonic}) - N_1(2 - \text{harmonic})}{N_1(4 - \text{harmonic})} \times 100, \tag{31}$$

where all steady-state values of N are calculated at $\xi = 12$. The results for the two models are shown in Fig. 5. It can be seen that for $R > 1$ (and all S values) and for $S < 0.2$ (and all R values) the difference between the numerical four-harmonic and the analytic two-harmonic predictions are less that 5% of the more accurate numerical result.

Comparing these results with the four-harmonic prediction presented in Fig. 3 makes clear that the disagreement becomes larger only when the sizes of the N_1 components are relatively small. The analytic models are not only accurate over three quarters of the range examined; more importantly, they are accurate over the range of parameters of most interest for practical holographic materials, namely, when $1 \leqslant R$.

7. APPLICATION TO EXPERIMENTAL DATA

In this section we estimate the physical parameters of the material by fitting experimental growth curves, using models I and II.

A. Polynomial Fits

Starting with the two-harmonic analytic solution for grating refractive-index modulation [Eq. (33b)], we find the Taylor series approximation to $n_1(\xi)$ close to $\xi = 0$, using relation (35b). The first three terms of this exact expansion are

$$\begin{aligned} &100CSf_1\xi - 25CSf_1[S(2f_0 + f_2) + 2f_0]\xi^2 \\ &\quad + \frac{25}{6}CSf_1\{4f_0^2 + (2f_0 + f_2)^2S^2 \\ &\quad + 2[f_1^2 + S(2f_0 + f_2)(f_0 + R)]\}\xi^3 \\ &\qquad = a_1^{\infty}\xi + a_2^{\infty}\xi^2 + a_3^{\infty}\xi^3 + \ldots . \end{aligned} \tag{32}$$

The n_1 experimental growth curves are produced from measured diffraction efficiencies corrected for Fresnel reflections.[22] In the experimental curves n_1 is plotted as a function of $I_0 \times t$, the exposure energy, and the polynomial fits to the experimental data are made in terms of this parameter:

$$\begin{aligned} n_1(I_0 \times t) &= e_1(I_0 \times t) + e_2(I_0 \times t)^2 + e_3(I_0 \times t)^3 \\ &\quad + \ldots + e_n(I_0 \times t)^n. \end{aligned} \tag{33a}$$

So the polynomial fit gives us the coefficients e_1, e_2, e_3, etc. In model II, however, $\xi = \kappa I_0^{1/2}t$. As we know the value of I_0 that was used during the fabrication of the gratings, we can compare like with like by rewriting Eq. (33a) in the form

$$\begin{aligned} n_1(I_0^{1/2} \times t) &= [e_1 \times I_0^{1/2}](I_0^{1/2} \times t) + [e_2 \times I_0](I_0^{1/2} \times t)^2 \\ &\quad + \ldots + [e_n \times I_0^{n/2}](I_0^{1/2} \times t)^n. \end{aligned} \tag{33b}$$

Equating the corresponding coefficients gives us that

$$[e_1 \times I_0^{1/2}] \cong a_1^{\infty}\kappa = 100CSf_1\kappa, \tag{34a}$$

$$[e_2 \times I_0^{2/2}] \cong a_2^{\infty}\kappa^2 = -25CSf_1[S(2f_0 + f_2) + 2f_0]\kappa^2, \tag{34b}$$

and so on.

First let us assume that the material response is local; i.e., that $\sigma \to 0$ and $S \to 1$. Then, from relations (34), κ can be estimated:

$$\frac{(e_2 \times I_0^{2/2})}{(e_1 \times I_0^{1/2})} \cong \frac{a_2^{\infty}\kappa^2}{a_1^{\infty}\kappa} = -\frac{4f_0 + f_2}{4}\kappa. \tag{35}$$

Therefore it is possible to determine a value for κ, given the experimentally extracted polynomial coefficients $(a_1^n\kappa)$ and $(a_2^n\kappa^2)$, from the fits to the experimental $n_1(I_0t)$ data curves. C can then be found, assuming that κ is already known, and a value for R can then be found by use of the values for κ and C.

Table 1 summarizes the resultant mean estimated values predicted for R, C, and κ from model II for various grating spatial frequencies. We first note the large variation in the parameter estimations. The values of κ found with model II were larger by an order of magnitude than those obtained with model I, whereas the C values were smaller by ~25%. We note the unphysical negative values of $R \sim -1.75$ found with model II, which are comparable with a small positive $R \sim +0.0223$ value estimated with model I.

Because $R = D_0K^2/F_0$ and K^2 is a function of the spatial frequency, the value of R should increase as the spatial frequency increases. Furthermore, C and κ are not functions of spatial frequency, so they should remain constant as the grating period changes. From Table 1 it can be seen that they do not appear to be constant when the growth curves are fitted by the use of polynomials. For these reasons this fitting technique was deemed unsatisfactory, and we decided to proceed by fitting the full curves, using the two-harmonic analytic formulas.

B. Two-Harmonic Analytic Function Fitting Technique

To fit the growth curves we used the model II expression for n_1 [Eqs. (29)]. By varying the values of R and S while keeping C and κ constant we obtained good agreement between experimental and theoretical curves. The fixed values assigned to κ and C were 0.035 $(m^2/W)/s$ and 1.9×10^{-5} L/mol, respectively. We arrived at these values through manual iteration, using as a starting point the values predicted from the polynomial fitting technique described in Subsection 7.A.

Table 1. R, C, and κ Extracted from Experimental Data with Model II Polynomial Fits

Spatial Frequency (lines/mm)	κ $(mW^{1/2})/s$	C [(L/mol) $\times 10^6$]	R
1000	3.028	2.13	−1.510
1250	2.345	1.93	−1.810
2000	2.414	1.42	−1.835
2250	2.522	1.51	−1.843
Mean	2.577	1.75	−1.750

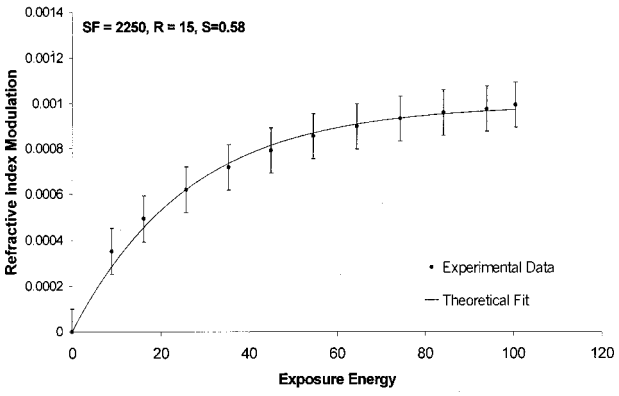

Fig. 6. Growth curve for spatial frequency 2250 lines/mm. Solid curve, analytic fit of two-harmonic Model II. Points, experimental data; error bars, $\pm 10^{-4}$.

Table 2. S, R, and $\sqrt{\sigma'}$ Obtained from the Model II Analytic Curve-Fitting Procedure

Spatial Frequency (lines/mm)	Λ (μm)	R	S	$\sqrt{\sigma'}$ (nm)
1000	1.0	3	0.95	51
1250	0.80	6	0.73	101
2000	0.50	12	0.62	77.8
2250	0.44	15	0.58	73.8
Mean				75.9

The growth of unslanted transmission gratings with different grating periods was monitored during exposure, and Fresnel reflection–corrected estimates of the resulting refractive-index modulation were extracted.[16–18] A model II analytic expression fitted to such a growth curve is shown in Fig. 6. The solid curve represents the theoretical fit achieved by use of the parameters shown; every tenth experimental data point is shown. The error bars represent the estimated uncertainty that is due to the acquisition system.[16] As can be seen, although they are not exact, the fits are reasonable. Table 2 lists the values of S and R that gave the best fits with the analytic two-harmonic model II curve-fitting procedure. Note that the value of R increases as the spatial frequency is increased, while the values of C and κ are held fixed. It can also be seen that, as would be expected, S decreases as the spatial frequency increases and the grating period, Λ, decreases.

Table 3 summarizes the trend in the value of R as the spatial frequency increases. The R values are found to follow the $R \propto 1/(I_0^{1/2}\Lambda^2)$ relationship predicted in the literature.[8–10] Furthermore, it was found that the experimental R values estimated with model II follow this theoretical relationship more closely than those found with model I. The diffusion coefficient was also estimated. For model II, $D = 3.31 \times 10^{-14}$ cm^2/s, which is almost the same as the value predicted by model I. It was found that R could be varied by as much as 15% and a good fit to experimental data still obtained. The quality of the fit is much more sensitive to the choice of values of S, which can be varied only by as much as 5% before the quality of the fit deteriorates markedly. This varia-

Table 3. Model II Changes in R for Increasing Spatial Frequency

Spatial Frequency (lines mm^{-1})	I_0 (mW)	$1/(I_0^{1/2} \times \Lambda^2) \times 10^{-11}$	R/R_{1000} (Experiment)	$\frac{I_0^{1/2} \times \Lambda_{1000}^2}{I_0^{1/2} \times \Lambda_{SF}^2}$ (Theory)
1000	3.825	5.11	1	1.00
1250	3.815	8.00	2	1.56
2000	3.763	20.6	4	4.03
2250	3.733	26.2	5	5.12

tion in S is equivalent to a 32.5% variation in σ. Outside these ranges of values of S and R the fits to the growth curves deteriorate, as does the agreement with the theoretical relationships.

8. CONCLUSION

In this paper we have generalized a nonlocal model, which we term model I,[8] to take into account any form of dependence of polymerization rate on intensity and used that generalized model to derive model II.[8] This generalization has been shown to be necessary[12,13] and related to fundamental physical parameters such as the quantum yield Φ within the photopolymer. The resultant numerical predictions of the four-harmonic models I and II have been compared. They most nearly agree when R is large ($R > 1$) and $S \rightarrow 1$ (local medium).

Two-harmonic analytic expressions based on model II have been presented and compared with the corresponding four-harmonic numerical predictions. The two-harmonic expressions have been shown to be accurate to within 5% for $R > 1$ (and all S values) and for $S < 0.2$ (and all R values). This range of validity should include many practical holographic recording materials.

Using the model II two-harmonic curve-fitting technique with $R \propto 1/(I^{1/2}\Lambda^2)$ and $\sqrt{\sigma'} = 75.9 \pm 25$ nm, we achieved satisfactory fits to experimental growth curves for an acrylamide-based photopolymer material with estimated values of $\kappa = 0.035\,(\mathrm{m/W^{1/2}})/\mathrm{s}$ and $C = 1.9 \times 10^{-5}$ L/mol. Diffusion coefficient D was calculated to be approximately 3.31×10^{-14} cm^2/s. The validity of these parameter estimates was discussed. It has been shown that the R values estimated with model II follow the theoretically expected behavior more closely than those found with model I.

The nonnormalized value for the nonlocal variance, $\sqrt{\sigma'} = 75.9 \pm 25$ nm, can be placed in the context of the length scales associated with general polymer chains. The length of a C–C bond is ~0.15 nm, and the carbon atom is ~0.1 nm long.[23] Therefore a repeat unit in a polyacrylamide chain of length ~0.5 nm would not be unexpected. Given that coiled polymer chains may contain from hundreds to tens of thousands of repeat units,[24,25] the lengths predicted by this model seem physically reasonable.

Although the analytic curve-fitting technique provides quite encouraging results, serious limitations of the method must be noted. The error bars associated with the experimental data and the resultant possible ranges of the estimated values of S and R indicate the crudeness of the estimates made. An improvement in the quality of the data and the use of an automated least-squares fitting procedure may overcome some of these difficulties.

Furthermore it was noted during application of the fitting procedures that the value for κ estimated from the analytic curve-fitting technique (Subsection 7.B) was an order of magnitude smaller than that estimated with the polynomial curve-fitting method (Subsection 7.A). The polynomial fits were carried out close to $\xi = 0$, and the analytic technique was used to fit the whole growth curve. This would suggest that the rate of polymerization is greater at the start of the exposure than at the end. Such a variable rate of polymerization is not allowed for in any of our models; however, it seems possible that such a rate may occur because at the start of polymerization there is much more monomer available to be polymerized.

Models were recently developed that describe photopolymer systems with more than one diffusing molecule (multicomponent systems).[26] We are currently developing coupled multiharmonic models, that incorporate these ideas. We are also exploring the affects of generalized nonlocal material response functions.[27] We would also bring to the reader's attention the recent Ref. 28.

J. T. Sheridan's e-mail address is john.sheridan@ucd.ie.

REFERENCES

1. W. S. Colburn and K. A. Haines, "Volume hologram formation in photopolymer materials," Appl. Opt. **10**, 1636–1641 (1971).
2. R. H. Wopschall and T. R. Pampalone, "Dry photopolymer film for recording holograms," Appl. Opt. **10**, 1636–1641 (1971).
3. R. T. Ingwall and M. Troll, "Mechanism of hologram formation in DMP-128 photopolymer," Opt. Eng. **28**, 586–591 (1989).
4. R. R. A. Syms, *Practical Volume Holography* (Clarendon, Oxford, 1990).
5. R. R. Adhami, D. J. Lanteigne, and D. A. Gregory, "Photopolymer hologram formation theory," Microwave Opt. Tech. Lett. **4**, 106–109 (1991).
6. G. Manivannan and R. A. Lessard, "Trends in holographic recording materials," Trends Polym. Sci. **2**, 282–290 (1994).
7. S. Piazzolla and B. K. Jenkins, "Holographic grating formation in photopolymers," Opt. Lett. **21**, 1075–1077 (1996).
8. J. T. Sheridan and J. R. Lawrence, "Non-local response diffusion model of holographic recording in photopolymer," J. Opt. Soc. Am. A **17**, 1108–1114 (2000).
9. P. W. Atkins, *Physical Chemistry*, 4th ed. (Oxford U. Press, Oxford, 1992).
10. G. Zhao and P. Mouroulis, "Diffusion model of hologram formation in dry photopolymer materials," J. Mod. Opt. **41**, 1929–1939 (1994).

11. V. L. Colvin, R. G. Larson, A. L. Harris, and M. L. Schilling, "Quantitative model of volume hologram formation in photopolymers," J. Appl. Phys. **81**, 5913–5923 (1997).
12. G. Zhao and P. Mouroulis, "Extension of a diffusion model for holographic photopolymers," J. Mod. Opt. **42**, 2571–2573 (1995).
13. G. Odian, *Principles of Polymerization* (McGraw-Hill, New York, 1970).
14. J. H. Kwon, H. C. Chang, and K. C. Woo, "Analysis of temporal behavior of beams diffracted by volume gratings formed in photopolymers," J. Opt. Soc. Am. B **16**, 1651–1657 (1999).
15. S. Martin, C. A. Feely, J. T. Sheridan, and V. Toal, "Applications of a self-developing photopolymer material: holographic interferometry and high efficiency diffractive optical elements," Opt. Memory Neural Netw. **7**, 79–87 (1998).
16. F. T. O'Neill, J. R. Lawrence, and J. T. Sheridan, "Automated recording and testing of holographic optical element arrays," Optik (Stuttgart) **111**, 459–467 (2000).
17. F. T. O'Neill, J. R. Lawrence, and J. T. Sheridan, "Thickness variation of a self-processing acrylamide-based photopolymer and reflection holography," Opt. Eng. **40**, 533–539 (2001).
18. F. T. O'Neill, J. R. Lawrence, and J. T. Sheridan, "Improvement of a holographic recording material using a aerosol sealant," J. Opt. A **3**, 20–25 (2001).
19. H. Kogelnik, "Coupled wave theory for thick holographic gratings," Bell Syst. Tech. J. **48**, 2909–2947 (1969).
20. L. Solymar and D. J. Cooke, *Volume Holography and Volume Gratings* (Academic, London, 1981).
21. S. Wolfram, *Mathematica*, 3rd ed. (Cambridge U. Press, Cambridge, 1996).
22. M. Born and E. Wolf, *Principles of Optics: Electromagnetic Theory of Propagation, Interference and Diffraction of Light*, 6th ed. (Pergamon, Oxford, 1980).
23. T. W. Graham Solomons, *Organic Chemistry*, 6th ed. (Wiley, New York, 1996).
24. M. Doi, *Introduction to Polymer Physics* (Clarendon, Oxford, 1997).
25. V. W. Krongauz and A. D. Trifunac, *Processes in Photoreactive Photopolymers* (Chapman & Hall, New York, 1994).
26. G. M. Karpov, V. V. Obukhovsky, T. N. Smirnova, and V. V. Lemeshko, "Spatial transfer of matter as a method of holographic recording in photoformers," Opt. Commun. **174**, 391–404 (2000).
27. J. T. Sheridan, M. Downey, and F. T. O'Neill, "Diffusion based model of holographic grating formation in photopolymers: generalized non-local material responses," J. Opt. A **3**, 477–488 (2001).
28. F. T. O'Neill, J. R. Lawrence, and J. T. Sheridan, "Comparison of holographic photopolymer materials using analytic nonlocal diffusion models," Appl. Opt. **41**, 845–852 (2002).